LUND UNIVERSITY
Faculty of Science

Calibration of Quenching for Laser-Induced Fluorescence of CO_2 at 2.7 μm

Philip Stjärneblad

Thesis submitted for the degree of Bachelor of Science
Project duration: 4 months

Supervised by Sebastian Pfaff and Johan Zetterberg

Department of Physics
Division of Combustion Physics
May 2019

Contents

Abstract

Knowledge about the gas-phase close to an active catalyst is essential in order to understand the properties of the catalytic reaction process. By the use of planar laser-induced fluorescence (PLIF), the gas-phase can be visualized with high spatial and temporal resolution without affecting the catalyst. In this work, catalytic CO oxidation over a Pd(100) catalyst is investigated using laser-induced fluorescence of CO_2. However, as the CO oxidation requires a gas mixture of CO, CO_2 and O_2, the problem of fluorescence quenching arises. This is caused by the CO_2 colliding with other molecules, where some energy transfers into kinetic energy. Therefore, a deeper study of the quenching factor is performed, it shows intensity drops of 50% as a result of quenching. Ultimately the quenching factors are applied to the Pd(100) measurement showing the gas-phase around the catalyst in greater detail.

1 Introduction

A catalyst is a material that provides chemical reactions with an alternative pathway. These pathways usually have a lower energy barrier, such that the reaction time is accelerated, and it does this without being consumed. For that reason, catalysis is widely used. In fact, catalysis is incorporated in the production steps of approximately 90% of all chemicals and material production in some way.

In addition to this, catalysis also presents opportunities to advance many different fields. In particular in the area of renewable energy, where new research in the field of photocatalysis has been conducted [1]. Here a direct functionalization of methane into ethanol has been proposed. This is an idea that if it where to be realized would present great value to society, as methane is one of the more radiative forcing gases in the atmosphere. Meaning that it increases the temperatures on earth by suppressing the energy that would otherwise radiate back out into space [2]. Advances in catalysis have already occurred, as three-way catalysts are used to clean toxic waste products in gasoline-fuelled vehicles. It does this by eliminating harmful exhaust gases, that of the CO, NO_x, and other hydrocarbons.

Many industrial catalysts have a complex composition and are active in harsh environments. For this reason, many reactions are very challenging to study, and thus many catalytic reactions are not fully known. Therefore, simplified models, such as a single crystal catalyst are useful as these present a window into the unknown. In these models, one is able to gain some fundamental knowledge about the active catalytic surface, as there is a well-defined surface within a single crystal. By extension, this well-defined surface enables us to study the influence of specific surface structures on the catalytic activity.

However, to fully comprehend the catalytic reactions one also has to account for the surrounding gas conditions. To that end, a simple reaction is commonly used as a model reaction during surface-science studies. CO oxidation presents itself as one of the most used for these kinds of studies, as it has been examined for several decades. Despite being studied extensively, the reaction is not yet entirely known for non-ultra-high vacuum (UHV) conditions. The reason for this is the number of molecules that interacts with the catalytic

surface increases rapidly with increasing pressure. Thus, knowledge about the gas composition at the catalyst surface is critical, as this knowledge would aid in the understanding of the gas–surface interaction.

To determine the gas composition close to the surface, several techniques are used simultaneously, namely mass spectrometry and laser-induced fluorescence [3]. In this way it is possible to obtain data at the same conditions with different instruments, giving a more detailed picture of the gas–surface interaction. By examining the gas composition with a mass spectrometer (MS), the activity of the catalyst is given, however, with low temporal resolution. Also, acceptable spatial resolution can be achieved by having a capillary close to the active catalytic gas-surface interaction, as this will minimize the path travelled by the gas molecules, allowing for detection of gas-phase molecules that are close to the catalyst surface.

Nevertheless, the spatial resolution of a mass spectrometer is limited to point measurements. For that reason, Planar laser-induced fluorescence (PLIF) is used to complement MS and provide a better spatial resolution. PLIF is an optical diagnostic technique that allows for instantaneous two-dimensional imaging of a gas phase and can thus be used to image the gas phase within a region close to the active catalyst [4].

With the introduction of fluorescence, the effects of molecular quenching arise as a problem. This affects the fluorescence intensity in such a way that gas concentrations are no longer represented in a linear fashion. In this work, the effect of quenching is examined, such that a calibration of the fluorescence signal of CO_2 can be determined. This calibration is then applied to a measurement of an active Pd(100) surface crystal, providing data with a more precise surface CO_2 composition.

2 Theoretical background

2.1 Laser

Light Amplification by Stimulated Emission of Radiation (LASER) is essential in the operation of PLIF. Starting in the framework of Bohr's model for the atom, one assumes the electrons only occupy discrete energy levels, such that one only requires two of these energy levels to derive the radiation law. The two levels denoted 1 and 2 are populated by a number of electrons N_2 in an excited state with an energy of E_2 and in the ground state there is a population of N_1 electrons with an energy E_1. In this way, the total number of electrons in the system is given by

$$N = N_1 + N_2 \tag{1}$$

To describe the transition between these states, one either needs emission or absorption of a photon. For emission, the electron in the excited state releases a photon with the energy $\Delta E = E_2 - E_1 = h\nu$ such that it can reach the ground state. This emission can occur in two ways, by spontaneous emission which happens when the electron randomly decays to the ground state, ejecting a photon in the process; or by stimulated emission, where the emission is instead caused by a passing photon with a specific wavelength. To fully

understand spontaneous emission one needs to turn to quantum electrodynamics, as it is ultimately caused by vacuum fluctuations in the quantized electromagnetic field [5].

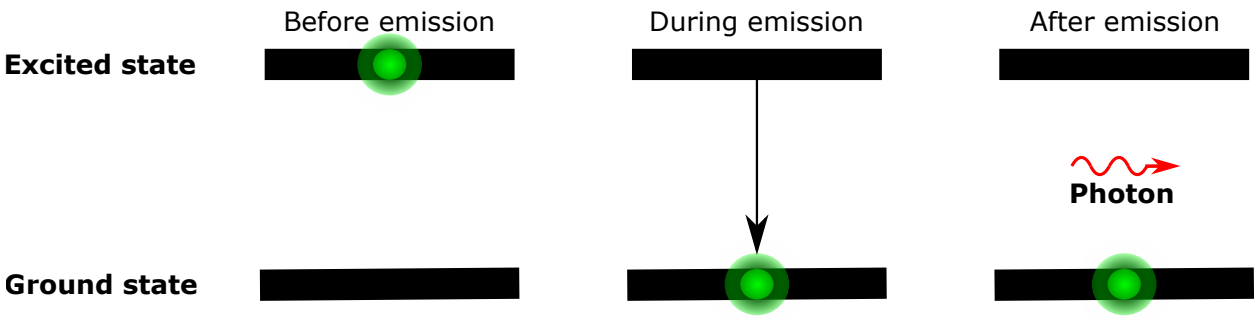

Figure 1: The event process during spontaneous emission.

As stated before, stimulated emission is caused by a passing photon with a specific wavelength. The passing photon interacts with the electron in the excited state, stimulating it to drop down into the ground state. In this way, it creates a new photon with the exact same properties as the passing one.

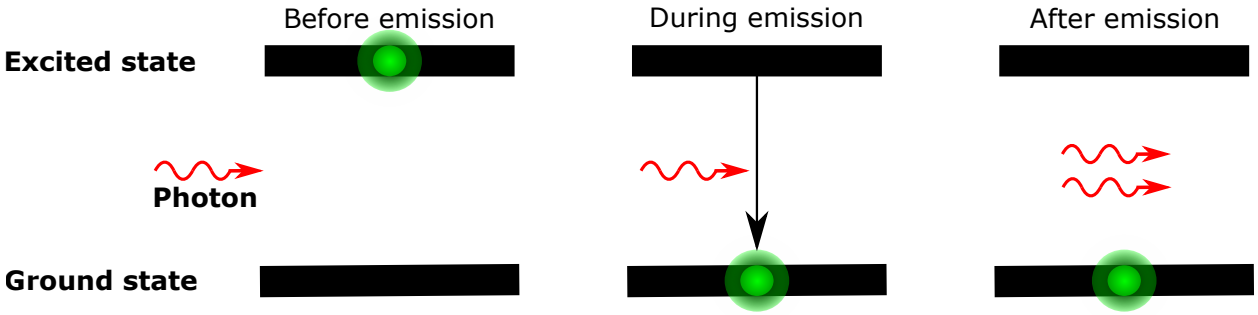

Figure 2: The event process during stimulated emission.

The transition rate for these events are given by,

$$\frac{dN_1}{dt} = A_{21}N_2 \tag{2}$$

$$\frac{dN_1}{dt} = \rho N_2 B_{21} \tag{3}$$

where A_{21} and B_{21} are constants known as Einstein's coefficients, ρ is the energy density of the radiation field. The last form of transition is absorption, which happens when a photon of specific energy is instead absorbed by the ground state electron, such that it goes to an excited state, and it has a transition rate of,

$$\frac{dN_2}{dt} = \rho N_1 B_{12} \tag{4}$$

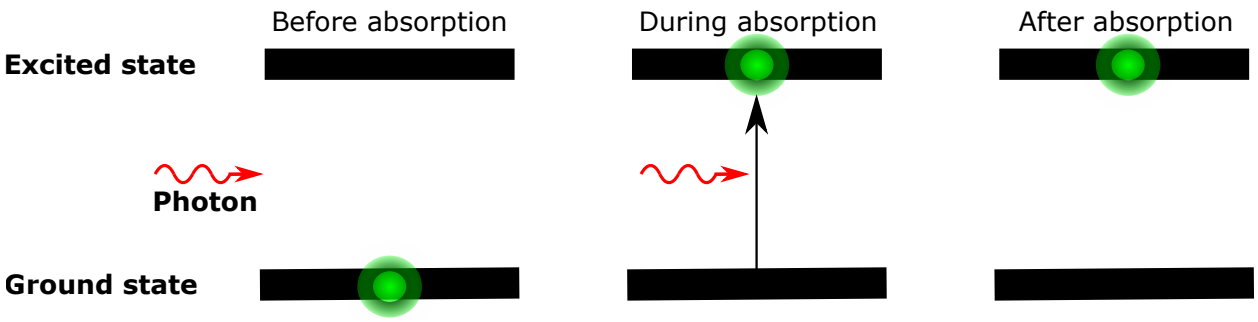

Figure 3: The event process during absorption.

While the system is in thermal equilibrium the transition rate between the two states are equal, such that,

$$\rho N_1 B_{12} = \rho N_2 B_{21} + A_{21} N_2 \tag{5}$$

Consider the states as being pumped out of the equilibrium by interactions with a light field of photon number n inside a resonator. By this there will be a gain and loss of electrons in the different states, these events have transition rates of, [6]

$$\frac{dN_2}{dt} = \Gamma N_1 \tag{6}$$

$$\frac{dN_1}{dt} = \gamma_{12} N_2 \tag{7}$$

where Γ and γ_{12} are constants. To get a functioning laser it needs at least three or more energy levels to obtain the desired population inversion. For that reason a Nd:YAG laser can be used, as the Nd:YAG material contains four energy levels which can seen be in fig.4.

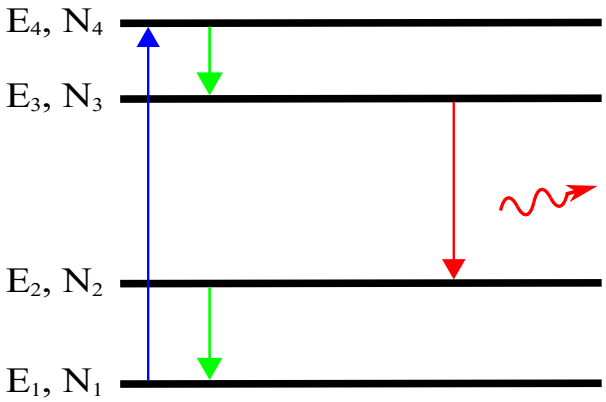

Figure 4: Optically pumping (blue arrow) the electrons from E_1 into E_4 via absorption. The electrons then undergo fast radiationless transfer (green arrow) down to the metastable state E_3. From E_3 the electron emits a photon, spontaneous emission, (red line) such that it goes down to E_2, where again it undergoes a non-radiative process down to the ground state.

Here the Nd:YAG metastable state E_3 is used to create the population inversion. To start the electrons are pumped from the ground state E_1 into "the pump state" E_4 and, as the lifetime of this state is on the order of picoseconds it will decay extremely quickly to the E_3.

This decay occurs via fast radiationless transfer, such that the energy difference is released without the emission of a photon.

As previously stated E_3 is a metastable state, and thus comparatively has a much longer lifetime than the other excited states. Therefore, new electrons will constantly come in from E_4, while the electrons in the metastable state are unable to leave at the same rate. Thus, the population of E_3 will increase rapidly and population inversion is achieved.

However, the electrons will ultimately go from E_3 down to E_2 given, enough time, and release a photon in the process. Again, the electron goes from E_2 to the ground state by fast radiationless transfer, and then the process is repeated. Now, the released photon has the possibility of stimulating an electron in another excited atom via stimulated emission. Therefore, these two photons can, in turn, stimulate other atoms such that a cascade of photons is released, hence an optical gain is created and the laser is operational [7].

2.2 Fluorescence

Fluorescence is a type of emission that occurs in a molecule after absorption of a photon, most commonly an electron in the ground state S_0 is excited into a higher electronic state S_1, as seen in fig.5. After the absorption, there is a non-radiative relaxation of the excited state on the picosecond scale, such that the state has a transition down to the vibrational zero level. This is the source of a slight energy difference between the absorption and fluorescence spectrum, as the wavelength of fluorescence emission sometimes will be longer as a result of the vibrational relaxation. Once the electron sits in the lowest vibrational level of S_1 it can go down to S_0 via the release of a photon. This process takes much longer time than that of the non-radiative process and the order of the relaxation time can be from a few nanoseconds up to hundreds of nanoseconds, depending on the relaxation pathway [8].

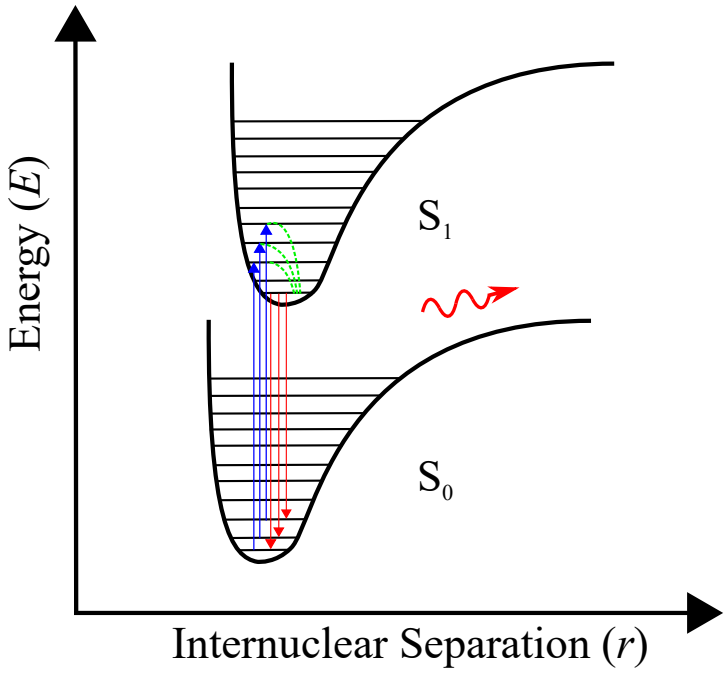

Figure 5: Schematic of two molecular states with vibrational levels. The blue arrows depict absorption of a photon, then the system relaxes from a higher vibrational level down to zero (green). Finally, the emissions of fluorescence are the red arrows

At first sight, even this energy shift might not seem sufficient to cause the dispersion between the absorption and emission. However, as the internuclear separation between the S_0 and S_1 is also shifted, there will be an overlap of different vibrational wave functions. As a result, the fluorescence emission has a higher probability of occurring between two vibrational energy levels in which the wave functions overlap. This vibronic transition rule is called the Franck–Condon principle and can be seen in fig.6.

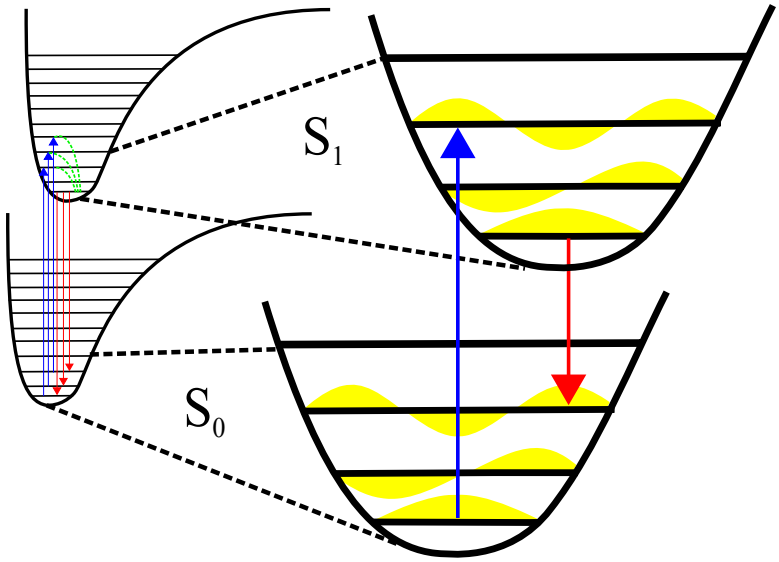

Figure 6: A diagram over the Franck–Condon principle, showing the vibronic wave functions of each state and how they overlap in a schematic way.

However, when this process involves more types of molecules i.e. a molecule M and Q, the possibility for quenching arises. Quenching causes a decrease in the fluorescence intensity as some of the energy will be lost through non-radiative processes. Some of these include collision with another atom or molecule, where energy is transferred into kinetic energy; electron transfer, where a donor and acceptor molecule would exchange an electron; energy transfer, this is possible if the absorption spectrum of the acceptor Q and the emission spectrum of the donor M overlaps, an example of this can be seen in fig.7 [8]. Among these possible quenching interactions, the most common one is through collision, as this does not require the molecules energy levels to overlap.

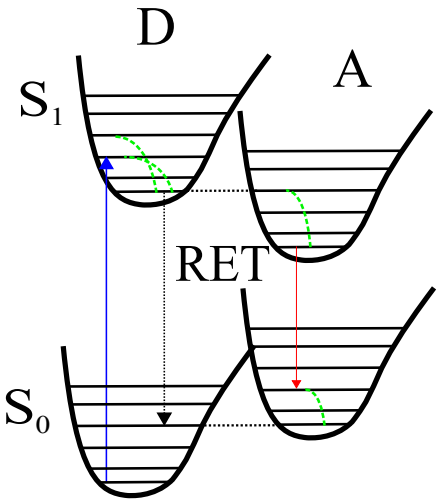

Figure 7: Schematic over an energy transfer, known as resonance energy transfer (RET) between two molecules. Here a nonradiative Coulombic interaction consisting of a dipole-dipole coupling cause the electron of the donor (D) to emigrate into the vibrational levels of the acceptor molecule (A).

3 Methodology

3.1 Experimental setup

To perform the PLIF measurements on CO_2 quenched by CO and O_2, the optical setup in figure 8 was used. A Q-switched Nd:YAG laser(Continuum, Powerlite DLS 8010), producing 1064-nm laser light with an energy of ∼350 mJ/pulse was used. The laser beam was then guided by optical mirrors into an infra-red Optical Parametric Oscillator (IR-OPO) (GWU, versaScan-L 1064) where it pumped a signal beam at a wavelength of ∼1.7 μm and pulse energy ∼8 mJ/ pulse, and an idler beam, at 2.7 μm with ∼7 mJ/pulse, both of which had a pulse duration of ∼5 ns.

As the signal and idler left the OPO, the two beams were separated by a dichroic mirror (HR at 2.7 μm). With the laser beams separated, a spherical CaF_2 lens (L1) at, $f = 500$ mm focused the beam; after-which approximately 10% of the laser energy got reflected onto a power meter, in order to see the energy variation on a shot-to-shot basis. To further enhance the signal strength, an N_2 filled tube along the laser path was used to reduce the energy loss

that otherwise would occur due to absorption by CO_2 in the ambient air. Furthermore, the beam was then formed into a thin laser sheet of ∼6 mm height by a cylindrical CaF_2 lens (L2), f = -40 mm and a spherical CaF_2 lens L3, f = 100 mm.

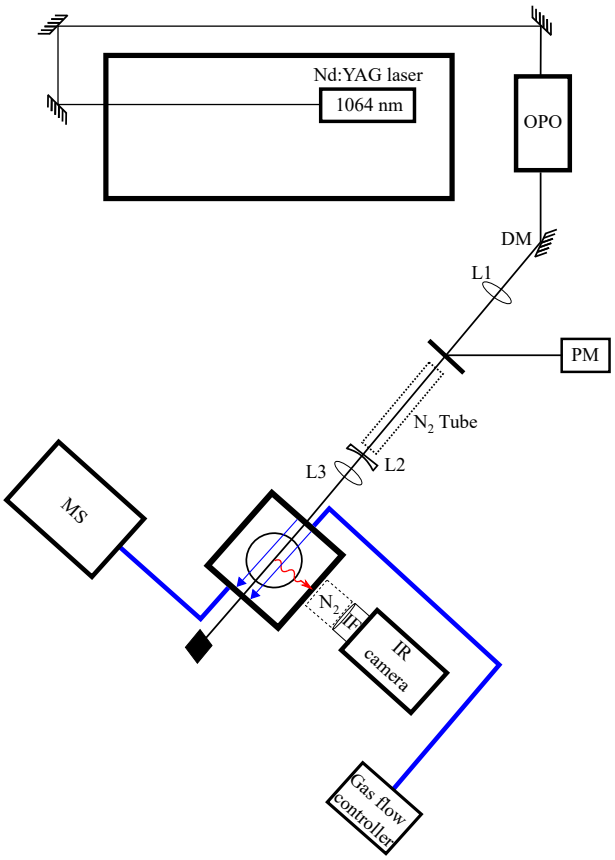

Figure 8: Schematic of the experimental setup. The laser light is first produced in an Nd:YAG laser, at 1064nm. Then the beam is directed into a Infra-red OPO Optical Parametric Oscillator where it pumps a signal beam and a idler beam. These are then separated in a DM dichroic mirror and focused by a CaF_2 lens $L1$, at f = 500 mm. The beam then passes a reflective mirror were approximately 10% of the laser energy is reflected onto a PM power meter. The rest of the beam passes a N_2 filled tube and two CaF_2 lenses, $L2$ at f = -40 mm and $L3$ at f = 100 mm. Once inside the reactor it excites the CO_2 molecules, producing fluorescences. This fluorescence then passes an N_2 filled tube and a IF interference filter, before reaching the IR camera. The gases inside the reactor are analysed using a MS mass spectrometer that is connected to the reactor.

With the beam focused it could induce fluorescence in the CO_2 within the reactor chamber. The gas flow in the chamber was provided by individual mass flow controllers (Bronkhorst EL-FLOW), and the pressure was controlled using an electronic pressure controller (Bronkhorst EL-PRESS). These allowed for digital control of the gas flow and pressure inside the chamber.

The chamber was equipped with a boralectric heater to control the sample temperature, as heat is needed to activate the catalysts. To allow for an approximative temperature monitoring of the sample, a type D thermocouple was connected to the side of the heater. Furthermore, to create well-defined boundary conditions around the reactor, it was also connected to a water-cooling system. In this way, the reactor walls were approximately the

same temperature throughout the data collection, as a side effect, it also decreased the cool down time of the reactor. Moreover, while measuring for catalytic reaction in the chamber the outflow gases would be analysed by a quadruple mass spectrometer (Pfeiffer, QME 220). However, for the case of the quenching measurements, there was no chemical reaction within the chamber, and instead the MS gave information about the gas stability in the chamber. This was of use as the gas controllers did not provide an instantaneous change of gas in the reactor, as there was some travel time in the gas tubing between the controllers and the chamber.

The emitted fluorescence was captured by a liquid-nitrogen-cooled, 256 × 256 InSb IR camera (Santa Barbara Focal Plane, SBF LP134) using a CaF_2 lens (f = 50 mm). The detection path was also purged with N_2 to reduce the signal loss of the fluorescence. The camera was set at an exposure time of 30 μs, in this way the entire fluorescence process is captured. Also, an additional 10 μs were set as a delay to the laser's q-switch, such to avoid scattering effects from the laser. To handle the varying thermal background radiation the camera was triggered at 20 Hz by a pulse generator (BNC, Model 575), where every other exposure where synchronized with the laser. As a result, an image with no induced fluorescence was captured every other exposure, so that the thermal background was obtained. This thermal background image could then be used to subtract the background from the image with induced fluorescence [4, 9, 10].

To control most of the experimental setup a digital LabVIEW interface was used, as it provided an easy and comprehensive graphical interface for the digital controls. The software allowed for remote control of the OPO, gas flow controllers and the boralectric heater, to name the most essential ones. Besides the active controls, it also enables real-time evaluation of the preliminary data, that of which came from the power meter, mass spectrometer and the thermocouples in the reactor. These were vital in order to assure that all instrument and conditions were stable prior to the collection of the fluorescence data.

4 Results and discussion

4.1 Quenching measurements

4.1.1 Excitation scan

Before collecting the main data, an excitation scan was performed on CO_2 by varying a stepper motor inside of the OPO. This slightly changed the OPO crystal angle, such that the photon energy distribution between the idler and signal beam was varied. In this way, one obtained the excitation spectrum of CO_2, as well as the preferred settings for the stepper, such that it gave the highest intensity for the LIF signal. This can be viewed in fig.9 where it was determined that the first peak gave the highest intensity. The peak was located at a stepper length of 7.650 cm that corresponded to a wavelength of ∼2681 nm.

Comparative data for the excitation scan was provided by HITRAN a high-resolution transmission molecular absorption database that provides spectroscopic parameters for prediction

and simulation of absorption spectra [11]. In this case, the excitation spectrum of CO_2 was acquired from the database, which was used to compare with the changing of the stepper to see the different molecular modes of CO_2 inside the chamber.

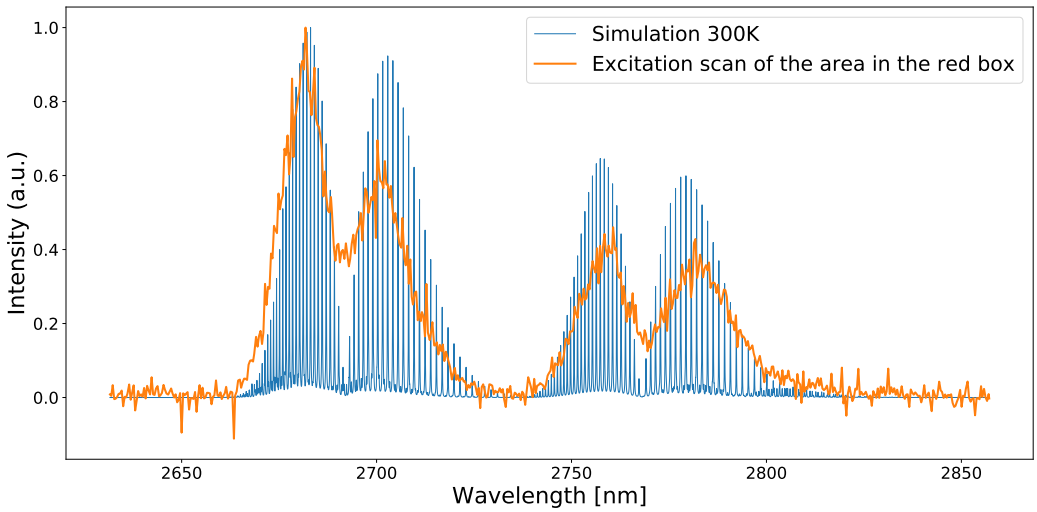

Figure 9: Renormalized simulation of CO_2 spectrum provided by HITRAN and the excitation scan of the area inside the red box fig.10 at ∼300 K.

4.1.2 Data collection

To examine the primary data, that of the fluorescence intensity of CO_2 that is quenched by CO and O_2. Here 2000 frames were acquired at each gas condition. Inside the chamber, the pressure was set to 150 mbar and with a constant gas flow of 100 ml/min. A reference image, henceforth profile image, was taken before each new gas change. To that end, three different profiles were collected at each temperature. The gas of the reference data was composed partially of a diluted mixture with 10% CO_2 and 90% Ar at a flow of 20 ml/min. The rest of the gas was purely Ar such to achieve the constant gas flow of 100 ml/min. Argon was picked as it is a noble gas, which helps to reduce some of the otherwise unpreventable quenching.

The first set of quenching measurements, those performed at ∼300 K, started with the gathering of the O_2 data followed by the CO and then finally CO and O_2 combined. These three were taken at gas flows between 0-5 ml/min and with steps of 0.5 ml/min, with again Ar as filler gas to get the desired constant gas flow of 100 ml/min and pressure of 150 mbar. To minimize experimental bias, the data was collected stochastically. In this way, one was able to avoid any other parameters, which could vary in a systematic way over time, influence the measurements. As for the measurements themselves, they were taken without much deviation from these set parameters. However, during the collection of data for O_2 at 3.5 ml/min some instabilities were encountered in the gas flow, as this fluctuated between 3.3 ml/min and 3.6ml/min. That said, the mean gas flow still was within the set parameter, ∼ 3.5 ml/min, yet this could prove to affect the result in some way. The ∼300 K measure-

ments was showing high stability throughout, as there were only slight intensity changes in the profiles. Also no sizeable variation in the mean shot to shot laser energy was present, as this was held at a stable rate throughout all measurements.

The second set of measurements was done at a temperature of ∼500 K, as this increased thermal energy could possibly affect the quenching by expanding the possible energy transfers. During the measurement, no instabilities in the set parameters were seen. However, the time for the chamber to reach thermal equilibrium had to be accounted for, and thus ∼5 minutes passed before the collection of the first profile. Nevertheless, it was later shown that this time was insufficient as the second profile deviated by 12% from the first one. The cause of this deviation most likely came from some disturbance in the laser energy or the wavelength, as it should have been sufficient time to reach thermal equilibrium. Despite this, the deviation was of little effect as the profiles were merely used to normalize the data. Also, as only intensity values close to the heater, fig.10, were used in the data evaluation the discrepancy was further mitigated.

As mentioned before, there is a constant thermal background that is being registered every second exposure. By subtracting this background from the laser shot image, one eliminates this effect. However, this is not the only aspect that has to be accounted for, as can be seen in fig.10 where the gas flow seemly bunches up into two separate forms. Thus, by directly viewing the intensity image, insight was gained on how the gas was distributed in the chamber. By knowing the distribution, a region of interest could be defined, giving more accurate quenching values.

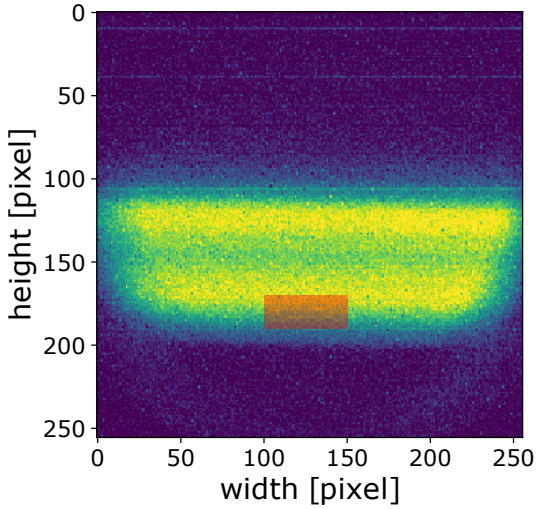

Figure 10: PLIF picture of a profile image at ∼300K, with the red shaded box indicating the area of interest for the data evaluation.

4.1.3 Quenching rates

Once the profiles and the concentration data had been taken for all of the different combinations, the mean value of intensity inside of the red box was taken in each individual image, such that each image provided an intensity value. Doing it this way, provided each mean intensity value with data from 70 000 pixels, minimizing the influence of laser fluctuations. Afterwards, the mean intensity values were plotted against their respective concentration. Finally, each gas combination was fitted with a (single-variable) quadratic function of the form,

$$f(x) = ax^2 + bx + c, \qquad a \neq 0 \tag{8}$$

as this function followed the trends of data reasonably well.

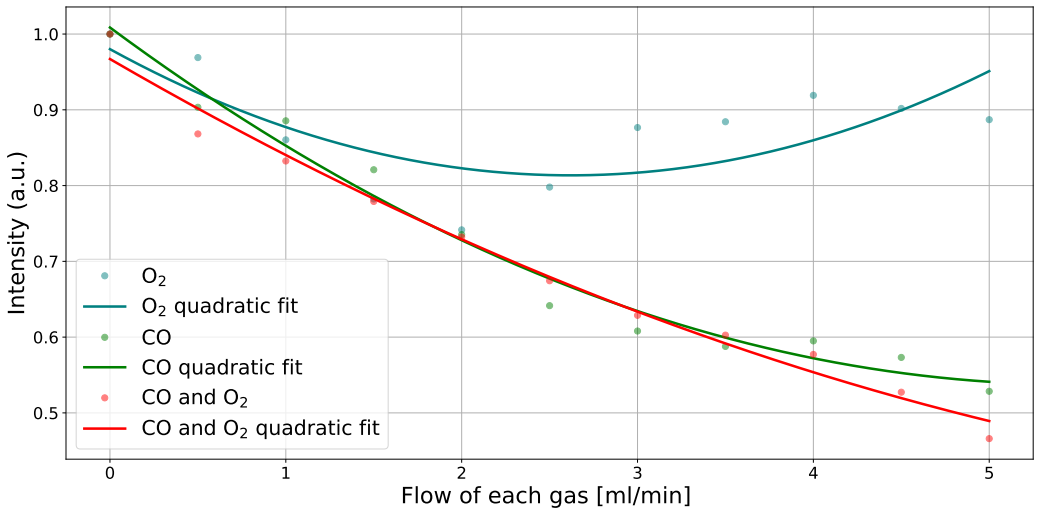

Figure 11: Quenching measurements for gases at ∼300K, with O_2 teal, CO green and CO, O_2 in red.

From fig.11 that of the ∼300K measurement, a few conclusions can be drawn. First, for O_2 the quenching rate seems to hit a maximum at ∼2.5 ml/min. This could indicate that at above 50/50 CO_2, O_2 concentration the quenching rate is reduced as a result of perhaps double energy transfer in intermolecular O_2 molecules. To determine the exact cause further investigation would be needed, as it currently stands without a definitive answer. Taking a step back, there are also some inconsistencies in the data between 3-4ml/min. This could be a result of the previously mentioned mass flows controller instabilities. However, no variation in the set values was seen during the collection of the data for these concentrations. Yet this could be the cause of the divergence from the other points. It is believed to be the result of some unwanted defect, as the anomaly was not visible in the ∼500K data, fig.12. This is further evident in the other gases as these overlapped quite well, no matter the temperature.

Furthermore, CO and CO, O_2 combined appear to follow a similar behaviour, with most of the quenching coming from the CO. Although, looking at the lowest and highest flows, O_2 does appear to have some impact on the quenching rate. Similarly, this is also supported

by the ∼500K data, albeit to a lesser extent. The results from both temperatures indicate that the increased thermal energy only has minimal effects on the quenching for all of the gases, but as the pressure was kept constant for both of the measurements the density during the ∼500K was higher. As a result, the quenching produced by collisions should be larger. That said it does appear to increase the quenching rate at higher flows, at least for CO. Again, this could also be a fault in the data as the change is small, and as peculiar variation occurred in O_2 for ∼300K it could be the case that this also happened elsewhere. However, there is nothing suggesting that any error developed throughout the collection of the data, as both the laser intensity and the gas flow controls were stable.

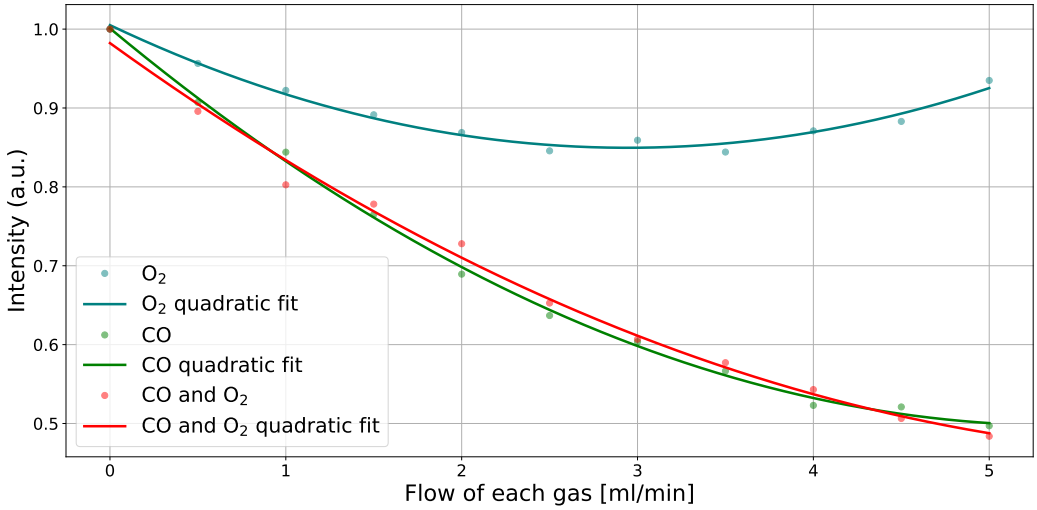

Figure 12: Quenching measurements for gases at ∼500K, with O_2 teal, CO green and CO, O_2 in red.

4.2 Quenching calibration on Pd(100)

4.2.1 Data collection

The Pd(100) activity data were collected at a separate occasion, and with different initial conditions. Firstly the experimental set-up was slightly changed by having the injected gas coming from the top of the rector instead of sideways. This helps in creating more well-defined gas flows at the catalytic surface, enabling easier modelling of the chamber. Also, the gas composition was changed to promote the needed reaction conditions. This gas composition consisted of 4 ml/min O_2, 4 ml/min CO and 0.2 ml/min CO_2 and Ar as a filler gas to receive a gas flow of 102 ml/min inside the chamber. A gas mixture that in hindsight could have been improved, as will be discussed later in section 4.2.2.

At first sight, the use of different gas flows, namely 102 ml/min for the catalytic cycle and 100 ml/min for the quenching calibration, might suggest that the environments are incomparable. However,as Ar is used to dilute the molecular gas the quenching rates will roughly stay the same. Thus, the different gas concentrations merely affects the intensity

and not the quenching rates. Hence, these gas concentrations can be approximated to be equal, as they quench roughly the same.

Other than these changes, the measurements were taken in a ramp. Meaning that the data collection started at ∼300 K and going up to ∼600 K in one interval, such that the catalytic activation became visible. Also, each measurement was preceded with the pumping of the chamber down to ∼1 mbar followed by a purging of the chamber with the set gases. The purging persisted for ∼5 min to rid the chamber of any residual gas that could have been present.

Onward, to that of data gathering, it was done by again collecting a profile with the same gas composition as in the quenching profile. However, the constant gas flow was 102 ml/min, and thus had more Ar dilution. Because the catalytic activation was examined, the boralectric heater was set to change between 0 A to 1.2 A during a 400 s interval. The camera collected 10000 frames to capture the entire heating interval. For the data with the catalyst subject to CO oxidation, these were taken in the same heating interval and with the same number of frames, but with changed gas composition. The stability for both runs was good, as no significant instabilities in gas flows or laser intensity were visible.

4.2.2 Calibration

In the data analysis, a few steps are required in order to use the quenching data to perform a calibration. Firstly, the quenching data has to be converted such that it depends on the concentration of CO_2. Additionally, as the gas mixture in the chamber is composed of CO and O_2 the quenching data of CO/O_2 at ∼300 K is used. Nevertheless, the pick of either the ∼300 K or the ∼500 K data set does not affect the calibration that much as both curves follow a similar gradient.

To start the derivation of the CO_2 dependency the following notations are important, as from now on C denote the real concentrations of CO_2 and C_m denote the measured concentrations of CO_2 that comes from dividing a measurement with a profile image. The quenching gas and the CO_2 concentrations are known within the quenching data, as is their dependency. Moreover, as a result of normalizing the data in fig.11. the y-axis can be given as function $q(C) = \frac{C_m}{C}$. Yet, as only C_m is known from the image one would like a certain C_m value to map to a quenching corrected C value. For that reason a new function $Q(C) = q(C)C$ is created, this calibration function provides the necessary components as it takes a value C_m and outputs a calibrated concentration C, see fig.13.

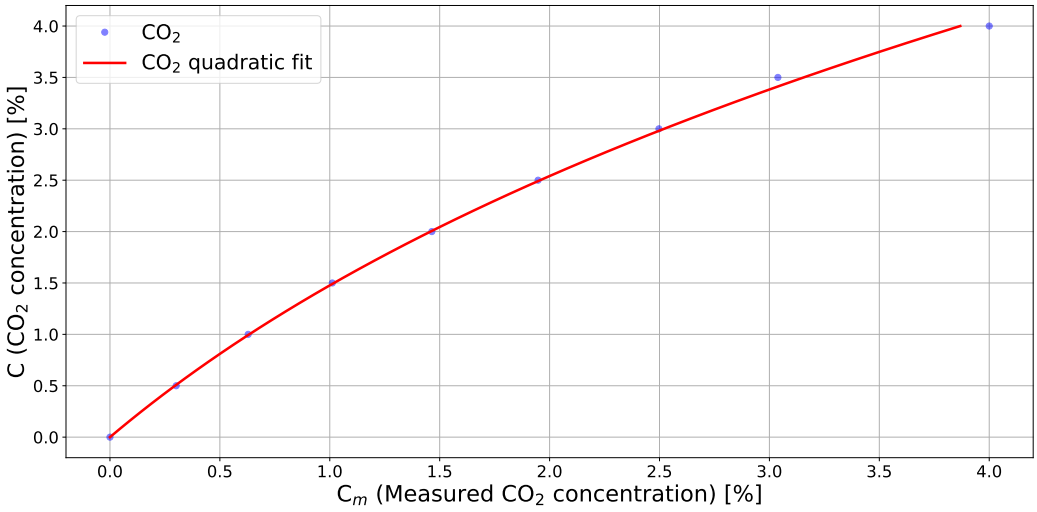

Figure 13: Diagram over the CO_2 concentration C as a function of the measured CO_2 concentration C_m

After creating the $Q(C) = q(C)C$ function the catalytic data could be calibrated. Although a few prerequisite steps were needed to fix the data. First, both the profile and the CO oxidation data were read and the thermal background that was captured every other exposure was subtracted from the laser shot images. Then the mean of 100 consecutive images was taken to remove intensity fluctuations. With this done, the CO oxidation data is divided with the profile in order to normalize it to create a corrected image. Despite being corrected it still lacks an essential piece of information, namely the scaling factor. This factor is given from the profile image, as it has known concentration of CO, O_2 and CO_2 inside of the chamber. The scaled image is displayed in fig.14. Furthermore, it is from this image the CO_2 intensity calibration is applied, as the quenching affects the fluorescence intensity of CO_2.

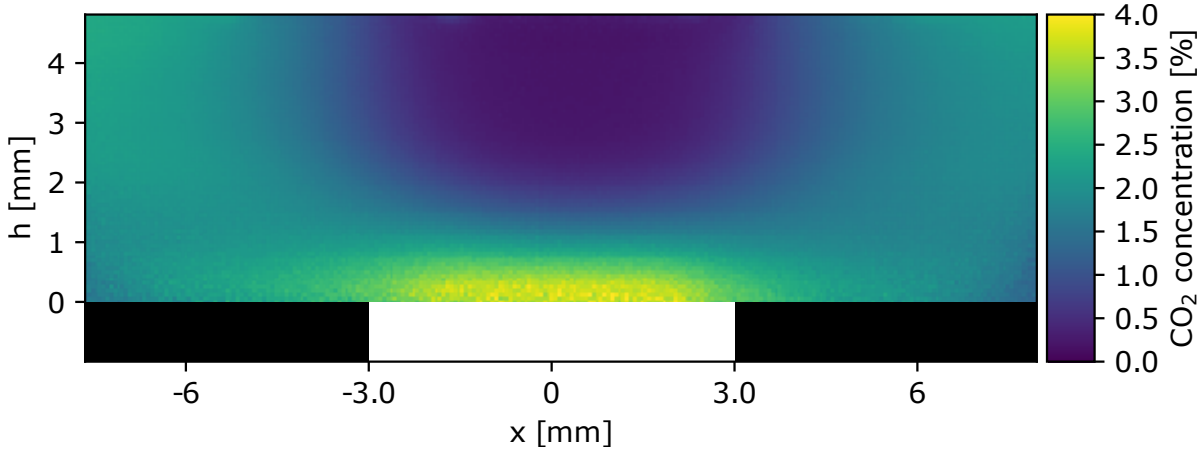

Figure 14: Image for the Pd(100) catalyst after the catalytic activation barrier has been crossed and without quenching calibration. Each pixel shows the measured concentration C_m of CO_2. Additionally the white bar under the image shows the location of the catalyst.

Consequently, the Pd(100) image without quenching calibration goes through the $Q(C) = q(C)C$ function, such that each pixel is adjusted according to its intensity. But the fact remains that the gas composition was not identical in the quenching measurement and the Pd(100) data and hence the quenching rates do not exactly simulate the catalytic measurements. Therefore, it could have been improved by either using the same gas flows or doing more extensive quenching measurements, as this would allow for a more realistic picture.

Moreover, an extension could be provided to this area of research by looking at how much the quenching rates are dependent on the filler gas, Ar, as currently it is only assumed to have little effect as a result of being a noble gas. Rather, it could affect the quenching from CO/O_2 by diluting the gas mixture to such a high extent that the fluorescence intensity from CO_2 is changed by preventing the energy transfer between the molecules as this only occurs at short distances. Even if improvements could have been done the result still shows great potential, as the intensity difference in fig.14 and fig.15 is clearly visible with improvements of 50% in some pixels. Besides the enhancements to this measurement, the calibration method will be used to improve future data where CO oxidation is examined.

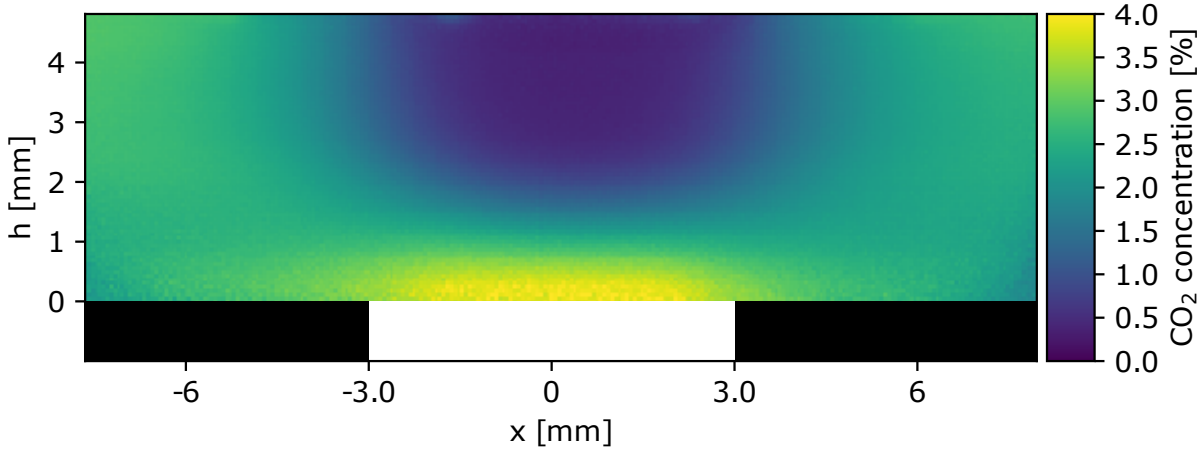

Figure 15: Image for the Pd(100) catalyst after the catalytic activation barrier has been crossed and with quenching calibration. Each pixel shows the corrected concentration C of CO_2, with the concentration being corrected by as much as 50% in some places. Additionally the white bar under the image shows the location of the catalyst.

5 Conclusions

Fluorescence quenching is an unavoidable effect while dealing with molecular gases and as new measurements need to be more accurate this effect needs to be calibrated for. The preformed measurement was therefore done to obtain some valuable data in order to better understand the CO oxidation, as fluorescence quenching is a problem. Indeed the data has shown that given a certain concentration quenching can reduce the perceived fluorescence intensity by as much as a factor of 50%. As a result, these measurements gave good ground for quantitatively determining the quench effects in CO and O_2 while operating the PLIF at a wavelength of $\sim$2681 nm. Quenching seems unaffected by increased temperature, at least for the examined temperature interval.

To get a more complete picture, another, more elaborate collection of data needs to be acquired. As currently, the effects of the filler gas argon, have been assumed to be negligible and have consequently not been fully taken into account. Additionally, it could be the case that it prevents the energy transfer between the molecules, such that it cannot simply be dismissed. To that end, an experiment in which a wide variety of different Ar concentrations are tested should be done, to see to what extent Ar affects the quenching.

Yet these improvements can only go so far, as there is some difference in the absorption rate of the PLIF-signal on the way to the camera. These rates will be a bit different from the profile to the actual measurement creating a direct error that is hard to correct. Also, there is a constant change of wavelength happening, even if the change is small, it is very difficult to adjust for, and as can be seen in the excitation spectrum cause quite a large shift in intensity.

That is why a more comprehensive way of correcting for these matters should be implemented. A possible way to do this is by the use of a reference cell, this cell would preferably have the same dimensions as the reactor and contain a known gas concentration. It should also have the same liquid-nitrogen-cooled, 256×256 InSb IR camera and a known fraction of the reflected laser beam. In this way, if the profile or reference data were to be collected simultaneously, most of these defects would be notably decreased, as the same laser light would induce fluorescence in the same way in both reference cell and the experimental chamber. In short, an additional camera, reactor and individual mass/pressure flow controllers should be implemented as it would allow for superior data collection.

6 Acknowledgements

I would like to thank my supervisor, Johan Zetterberg, for providing me with the opportunity to be a part of this project. Many thanks to my Co-supervisor Sebastian Pfaff, who first introduced me to the work done at Combustion Physics and allowed me to participate in his work. In addition, he also helped me immensely by answering my stupid questions and teaching me many new concepts. We also had good discussions, and he gave me clear instructions, sparking my interest in the subject. As, if this was not enough, he would also provide me with friendship, that hopefully will last long after my departure from the department.

References

[1] Y. Zhou, L. Zhang, and W. Wang. Direct functionalization of methane into ethanol over copper modified polymeric carbon nitride via photocatalysis. *Nature communications*, 10(1):506, 2019.

[2] M. Etminan, G. Myhre, E. J. Highwood, and K. P. Shine. Radiative forcing of carbon dioxide, methane, and nitrous oxide: A significant revision of the methane radiative forcing. *Geophysical Research Letters*, 43(24), 2016.

[3] J. Zhou, S. Pfaff, E. Lundgren, and J. Zetterberg. A convenient setup for laser-induced fluorescence imaging of both CO and CO_2 during catalytic CO oxidation. *Applied Physics B*, 123(3):87, 2017.

[4] S. Blomberg, J. Zetterberg, J. Gustafson, J. Zhou, M. Shipilin, S. Pfaff, U. Hejral, P. A. Carlsson, O. Gutowski, F. Bertram, and E. Lundgren. Combining synchrotron light with laser technology in catalysis research. *Journal of synchrotron radiation*, 25(5), 2018.

[5] H. Yokoyama and K. Ujihara. *Spontaneous emission and laser oscillation in microcavities*, chapter 1, page 6. CRC press, 1995.

[6] F. Grossmann. *A Short Introduction to Laser Physics*, pages 3–15. Springer International Publishing, Heidelberg, 2013.

[7] A. Goyal and M. Goyal. *Diode Pumped Nd:YAG Laser*. ALKAAD Photonics, 12 2014. An optional note.

[8] B. Valeur. Molecular fluorescence. *digital Encyclopedia of Applied Physics*, pages 477–531, 2003.

[9] J. Zetterberg, S. Blomberg, J. Gustafson, J. Evertsson, J. Zhou, E. C. Adams, P. A. Carlsson, M. Aldén, and E. Lundgren. Spatially and temporally resolved gas distributions around heterogeneous catalysts using infrared planar laser-induced fluorescence. *Nature communications*, 6:7076, 2015.

[10] J. Zetterberg, S. Blomberg, J. Gustafson, Z. W. Sun, Z. S. Li, E. Lundgren, and M. Aldén. An in situ set up for the detection of CO_2 from catalytic CO oxidation by using planar laser-induced fluorescence. *Review of scientific instruments*, 83(5):053104, 2012.

[11] I. E. Gordon, L. S. Rothman, R. V. Hill, C.and Kochanov, Y. Tan, P. F. Bernath, M. Birk, V. Boudon, A. Campargue, K. V. Chance, et al. The hitran2016 molecular spectroscopic database. *Journal of Quantitative Spectroscopy and Radiative Transfer*, 203:3–69, 2017.